PS Kinematics and Growth of Supra-Salt Systems: A Field and Subsurface Analysis, Paradox Basin*

Elizabeth Horne[1] and Bruce Trudgill[1]

Search and Discovery Article #30515 (2017)**
Posted August 21, 2017

*Adapted from poster presentation given at 2017 AAPG Annual Convention & Exhibition, Houston, Texas, April 2-5, 2017

[1]Colorado School of Mines, Golden, Colorado (elilyhorne@gmail.com)

Abstract

Salt can provide the structure and seal necessary for hydrocarbon entrapment, however, it may lead structural complexities, such as compartmentalizing a hydrocarbon reservoir through supra-salt faulting. Outcrop analog studies provide exceptional opportunities to observe how salt-influenced fault geometries evolved spatially and temporally. The Paradox Basin in southeastern Utah is an example of a salt-influenced petroleum basin where the petroleum system is directly associated with evaporites. Decades of petroleum exploration in the region have yielded in a broad subsurface dataset (e.g. seismic reflection data and well penetrations), with close proximity to world-class outcrops. Exposed supra-salt fault scarps have preserved kinematic evidence which provide tangible evidence to populate kinematic models that quantify the temporal and spatial evolution of this fault system.

This study focuses on the Salt Valley salt wall, the northernmost and largest salt structure within the northern Paradox Basin. A 40 km long supra-salt fault array trends parallel to and detaches downward onto the NW-plunging salt wall. Through the use of 3D seismic reflection data, wells, published maps, satellite imagery, and a collection of structural field measurements, we are able to build a database that was used to make an integrated interpretation of the spatial and temporal evolution of the fault array.

Several kinematic analyses coupled with detailed geometric fault descriptions were used to determine the growth history of the studied fault array that consists of a series of overlapping fault segments up to 12.5 km long, with throws of hundreds of meters, defining a series of crestal grabens and half-grabens. Secondary faults of similar length are present on the flanks of the salt wall. Along the strike of the fault array, there are notable changes in the dip direction of the half-graben master faults and regions of varying fault strikes. These changes reflect heterogeneities of the top-salt geometry.

Fault linkage analyses such as: fault throw-length (T-L); throw-distance (T-x); throw-depth (T-z), as well as qualitative distribution of fault throws from map and strike views show that these segments are over-displaced, with a complex fault segment linkage history. We hypothesize that these over-displaced faults evolved with a hybrid fault growth model, where they initiated as isolated fault model but spent the majority of their growth history through coherent fault growth.

Abstract

Salt can provide the structure and seal necessary for hydrocarbon entrapment, however, it may lead structural complexities, such as compartmentalizing a hydrocarbon reservoir through supra-salt faulting. Outcrop analog studies provide exceptional opportunities to observe how salt influenced fault geometries evolved spatially and temporally. The Paradox Basin in southeastern Utah is an example of a salt-influenced petroleum basin where the petroleum system is directly associated with evaporites. Decades of petroleum exploration in the region have yielded in a broad subsurface dataset (e.g., seismic reflection data and well penetrations), with close proximity to world-class outcrops. Exposed supra-salt fault scarps have preserved kinematic evidence which provide tangible evidence to populate kinematic models that quantify the temporal and spatial evolution of this fault system.

This study focuses on the Salt Valley salt wall, the northernmost and largest salt structure within the northern Paradox Basin. A 40 km long supra-salt fault array trends parallel to and detaches downward onto the NW-plunging salt wall. Through the use of 3D seismic reflection data, wells, published maps, satellite imagery, and a collection of structural field measurements, we are able to build a database that was used to make an integrated interpretation of the spatial and temporal evolution of the fault array.

Several kinematic analyses coupled with detailed geometric fault descriptions were used to determine the growth history of the studied fault array that consists of a series of overlapping fault segments up to 12.5 km long, with throws of hundreds of meters, defining a series of crestal grabens and half-grabens. Secondary faults of similar length are present on the flanks of the salt wall. Along the strike of the fault array, there are notable changes in the dip direction of the half-graben master faults and regions of varying fault strikes. These changes reflect heterogeneities of the top-salt geometry.

Fault linkage analyses such as: fault throw-length (T-L); throw-distance (T-x); throw-depth (T-z), as well as qualitative distribution of fault throws from map and strike views show that these segments are over-displaced, with a complex fault segment linkage history. We hypothesize that these over-displaced faults evolved with a hybrid fault growth model, where they initiated as isolated fault model but spent the majority of their growth history through coherent fault growth.

Research Objectives

(1) Produce a detailed geologic map of the Salt Valley salt wall

(2) Build a water-tight 3D structural framework of the subsurface Salt Valley salt wall

(3) Identify geometric similarities between surficially-mapped and subsurface faults

(4) Conduct throw distribution studies on linked subsurface fault zones to determine fault growth histories

(5) Advance understanding of the spatial and temporal evolution of the supra-salt fault array in Salt Valley

(6) Conduct statistical analyses to identify style of deformation and mechanism of fault initiation

Motivation

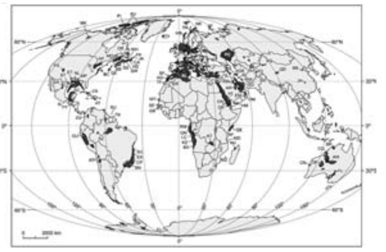

Equal-area Mollweide projection showing global distribution of basins containing salt structures (dark-gray polygons) (Hudec and Jackson, 2007).

Many of the world's largest hydrocarbon provinces are present within salt basins (e.g., Gulf of Mexico, North Sea, Persian Gulf, Campos Basin and Pricaspian Basin) (Hudec and Jackson, 2007).

Evaporitic minerals, such as halite (NaCl), possess unique physical and chemical properties which can affect multiple aspects of a petroleum system (i.e., thermally conductive, incompressible, diffusive, etc.). Salt is mechanically weak at shallow depths and accommodates strain and displacement through ductile flow (Hudec and Jackson, 2007).

These volumes can:
- Form décollements
- Decouple sub- and supra-salt faulting (Morley et al., 2003)
- Inhibit the lateral and vertical propagation of faults (Richardson et al., 2005)
- Impact the presence, stratal geometry and distribution of sedimentary systems (Giles and Lawton, 2002; Kluth and Duchene, 2009; Hearon, 2013)
- Control timing of source maturation
- Provide seal for fluid migration (Hudec and Jackson, 2007)

Location map of the Paradox Basin, Utah, Colorado, Arizona and New Mexico showing producing oil and gas fields, the Paradox fold and fault belt, and Blanding sub-basin as well as surrounding Laramide basins and uplifts. Modified from Harr, 1996.

The Paradox Basin in SE Utah is a salt-influenced petroleum basin where the petroleum system is directly associated with evaporites.

Small-scale petroleum production is present throughout the basin with a majority of production in the southwest (Stevenson and Wray, 2009).

As a result, the entire basin has been subjected to different levels of petroleum exploration (e.g., 2D & 3D seismic reflection data collection, wild-cat well penetrations), adjacent to world-class outcrops.

Geologic Context

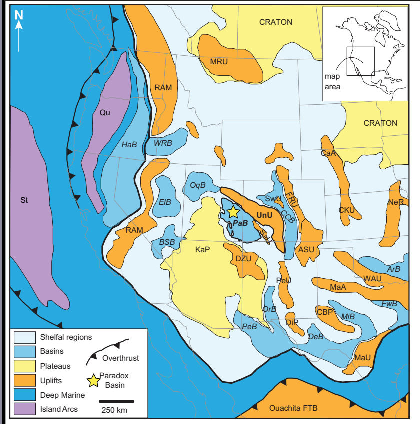

Paleogeographic and plate tectonic reconstruction of western North America during the middle Pennsylvanian (~310 Ma) Modified from Trudgill, 2011.

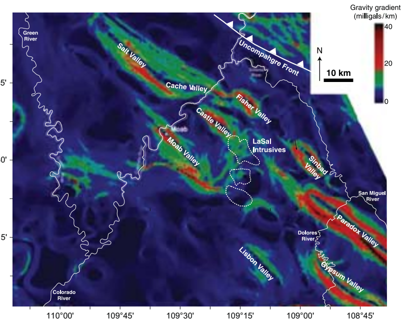

Gravity gradient map from (Banbury, 2005) after data from Case and Joesting (1972), modified from (Trudgill, 2011).

The Paradox Basin is an asymmetric foreland basin that developed during the Ancestral Rocky Mountain orogeny during the Late Pennsylvanian – Permian (Barbeau, 2003).

This basin is characterized by a vast volume of evaporites (up to ~2500 m) that were deposited within the subsiding footwall of the Uncompahgre Uplift. Rapid deposition of clastic material shed from the Uncompahgre Uplift mobilized Paradox evaporites into elongate, diapiric, salt walls that trend subparallel to the northwest-trending thrust front.

These accumulations are recognizeable in gravity gradient maps and aerial extents have been documented in published maps and cross sections.

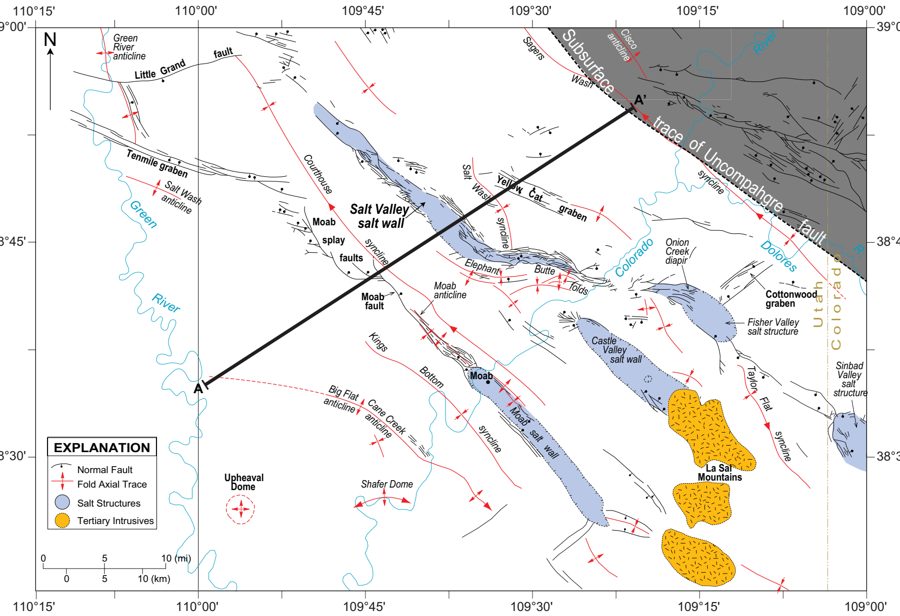

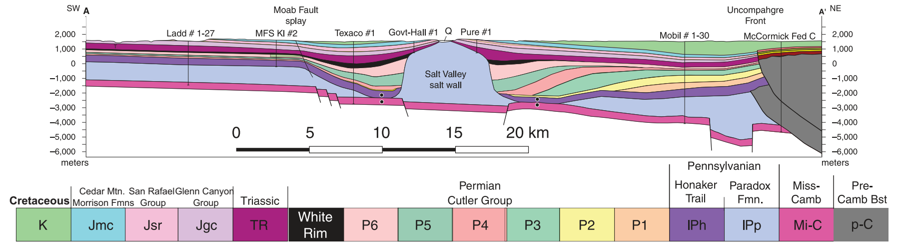

Location map of northern Salt Anticline region of the Paradox Basin. The bold black line highlights the approximate location of cross-section A-A', which illustrates stratigraphic architecture and salt wall geometries in the northern Paradox basin. Light blue polygons highlight evaporite bodies in both map and cross-section.

Map after Doelling, 1983; Trudgill et. al. 2004; modified from Trudgill and Arbuckle, 2009 and Lehmann, 2015. Cross-section modified from Trudgill, 2011.

Tectonic Evolution of the Paradox Basin

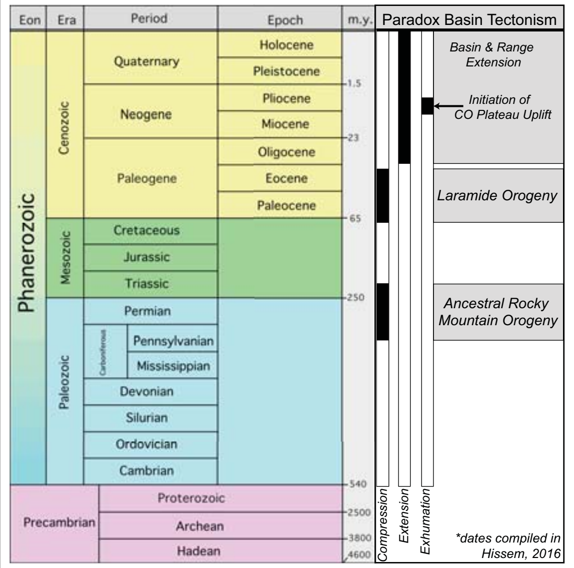

Prior to the Ancestral Rocky Mountain orogeny, this region underwent crustal extension in the Proterozoic. This extension resulted in the formation of northwest trending basement-involved faults that were subsequently reactivated during Pennsylvanian-Permian Ancestral Rocky Mountains.

The Laramide orogeny in the Late Cretaceous to early Eocene is responsible for much of the deformation in western North America. Though several structures formed and were reactivated in this event, (e.g., the Uncompahghre thrust and the San Rafael Swell) the Laramide fold and fault belt bypassed much of the Colorado Plateau (Barbeau, 2003). Specifically, it is thought that the principal structures of the Paradox Basin show negligible amounts of structural disturbance from the Laramide, and more importantly, the salt structures were amongst the least affected from this compressional period (Barbeau, 2003)

Uplift of the Colorado Plateau initiated in the Miocene, overlapping with Basin and Range extension

The aerial limits of the elongate salt walls are coincident with presalt structures. Precambrian basement normal faults bound these walls to the northeast and southwest with secondary, northeast-trending basement fabric that further compartmentalizes the extent of the salt walls (Hite, 1975; Warner, 1978).

Methods and Analyses

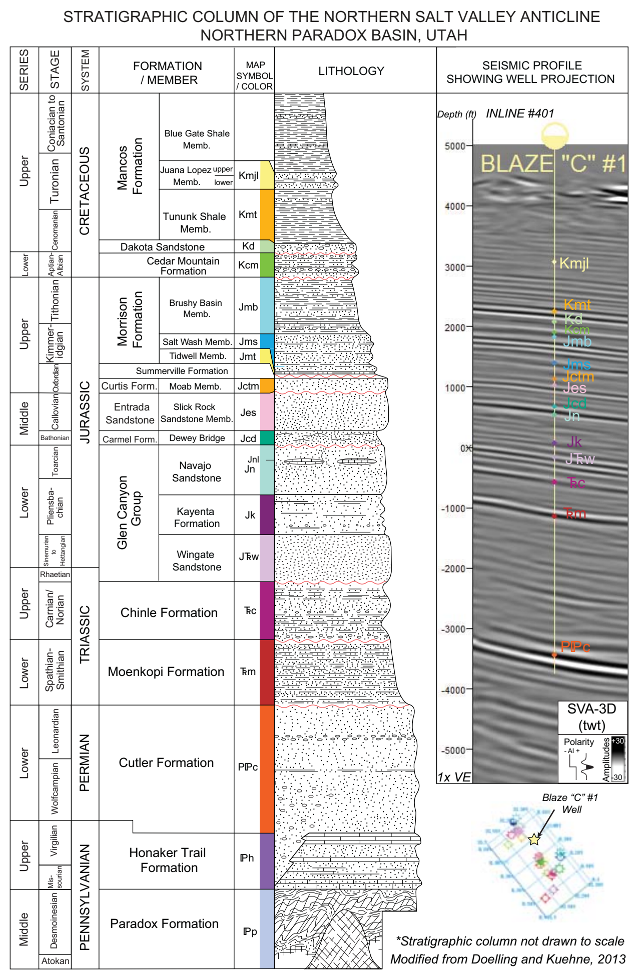

3D Framework Modeling

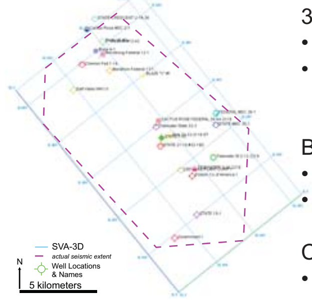

Database:

3D Seismic Survey (18.1 km2)
- 541 inlines
- 328 crosslines
  - Line spacing: 33.5 m (110 ft)

Borehole data (23 wells)
- Most contain basic wireline log and checkshot surveys
- *Very sparse TD data*

Cultural Data:
- Published maps & cross-sections (geotiffs, shapefiles)
- High-resolution aerial imagery
- Digital elevation models (DEM's)

Subsurface Methods:

3D seismic interpretation
1) Seismic attribute analysis
   Enhance acoustic impedance contrasts to better image: horizon reflectors, voids created by faulting, and top-salt surface
2) Fault interpretations
   - Fault geometries/ detachment surfaces
   - Locations displaying fault segment link-up
3) Horizon interpretations
   - Gridded horizons
   - Identify growth strata
   - Top-salt geometry & heterogeneities
4) Construct 3D Structural Framework
5) Generate velocity model for depth conversion

Subsurface Analyses

Static structural characterization of the SVA suprasalt fault system
1) Structural Orientations
2) Fault length vs. throw distribution
3) Fault throw vs. depth
4) Changes in throw gradients along strike

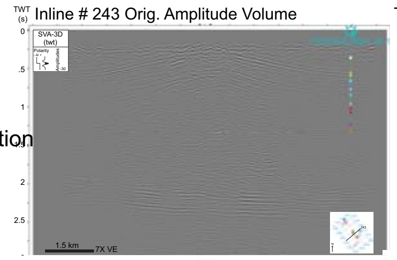

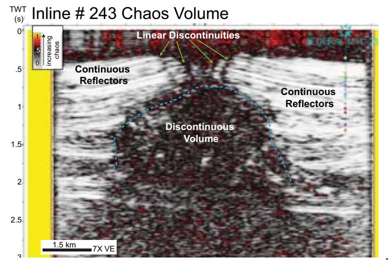

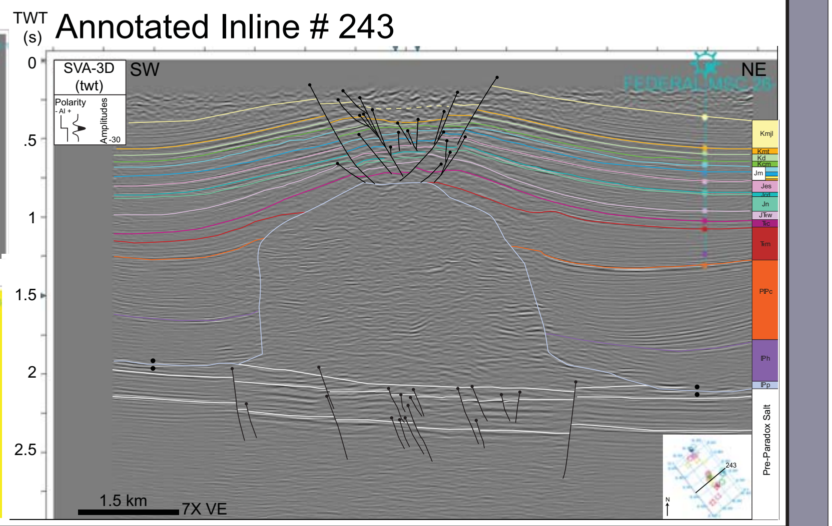

Field Mapping

Panoramic view the northeastern margin of the salt valley salt wall. This image captures typical outfopping patterns and geometries of Mesozoic strata, as well as exhibits ... ability to map in the field... lithologies on

Methodology:

Collect key structural measurements:
- Strike & dip
  - Bedding
  - Fault surfaces
- Trend & plunge
  - Slikenlines

* Measurements compiled into stereonet diagrams to identify paleo-stress orientations and kinematic axes

- Documentation of exposed stratigraphic contacts
- Record changes in facies and unit thicknesses
- Compare to published maps & structural measurement's
- Integrate collected field data with subsurface framework
- Photography of key outcrop exposures

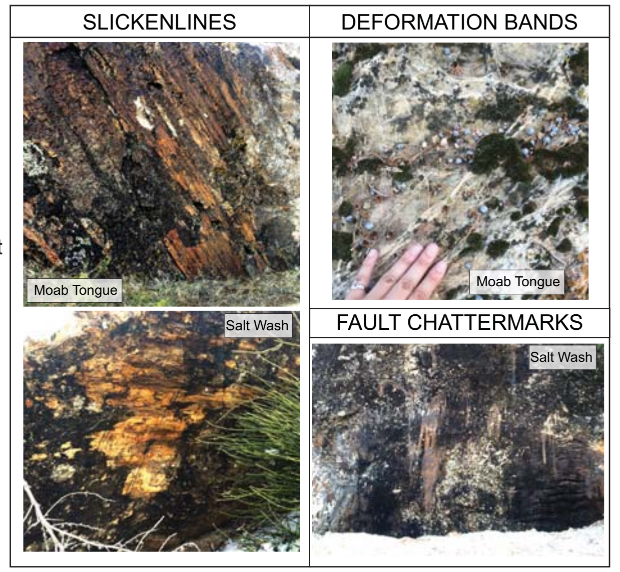

Field photos highlighting various outcropping structures.

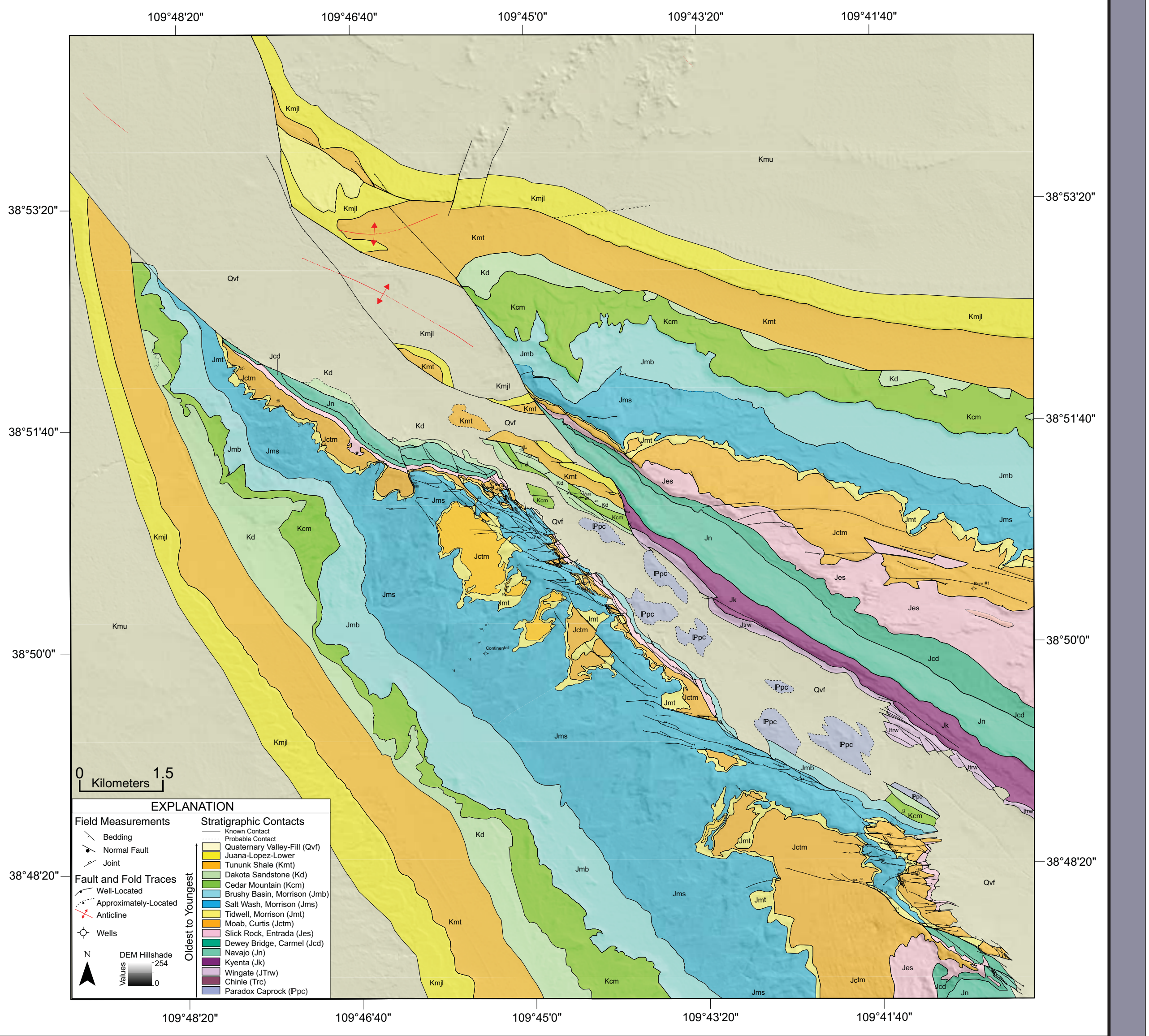

Kinematics and Growth of Supra-Salt Fault Systems: A Field and Subsurface Analysis

Elizabeth Horne[1], Bruce Trudgill[1]
[1]Colorado School of Mines, Golden, CO
Email: elilyhorne@gmail.com

COLORADO SCHOOL OF MINES
EARTH • ENERGY • ENVIRONMENT

Surface Structure Maps

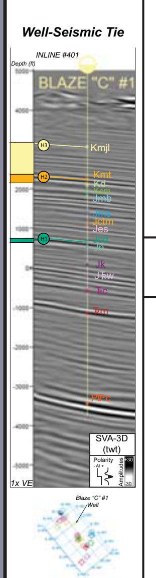

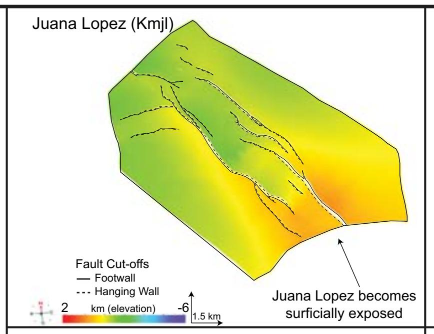

Surface structure map of the Juana Lopez Member of the Cretaceous Mancos Formation.

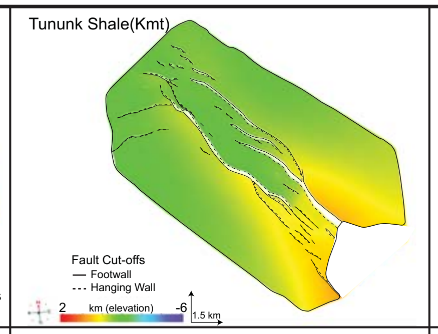

Surface structure map of the Tununk Shale Member of the Cretaceous Mancos Formation.

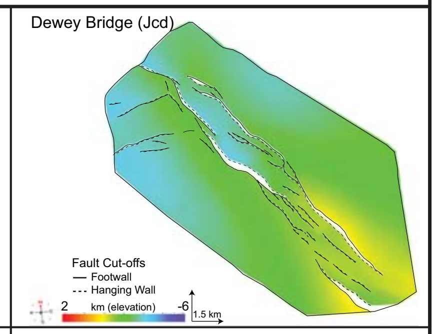

Surface structure map of the Dewey Bridge Member of the Jurassic Curtis Formation.

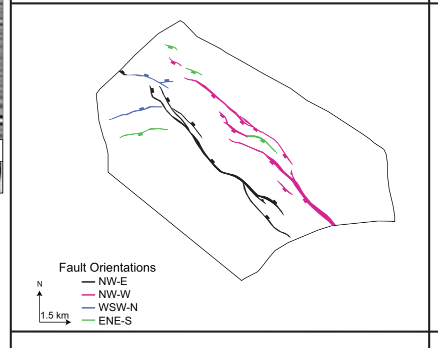

Orientations of faults that intersect the Juana Lopez Member of the Cretaceous Mancos Formation.

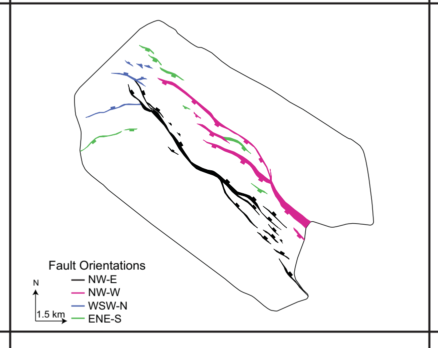

Orientations of faults that intersect the Tununk Shale Member of the Cretaceous Mancos Formation.

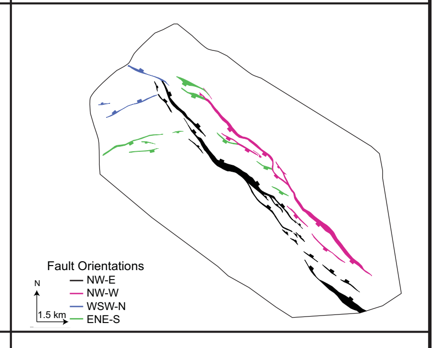

Orientations of faults that intersect the Dewey Bridge Member of the Jurassic Curtis Formation.

Supra-Salt Fault Array

Supra-Salt Fault Array

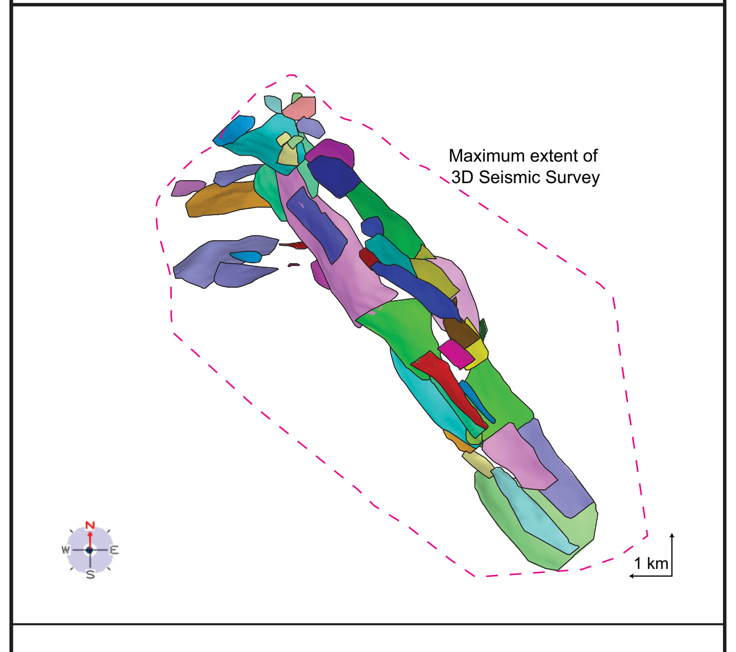

Aerial view of all faults mapped using the 3D SVA seismic survey. The pink dashed polygon represents the maximum extent of 3D seismic data. Colors are chosen at random to illustrate independent fault surfaces.

Strike Orientations

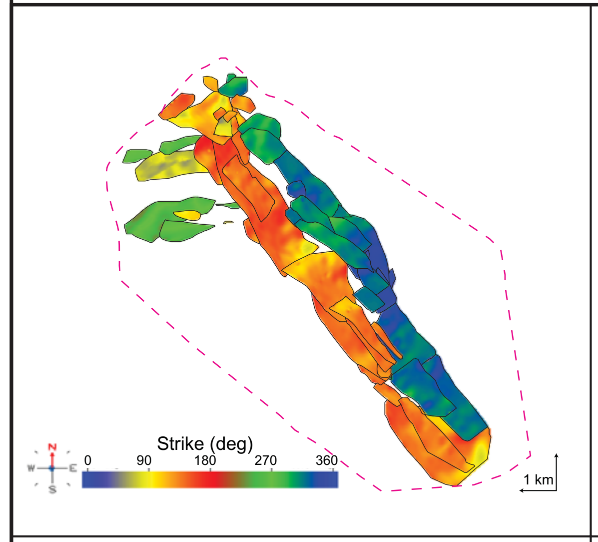

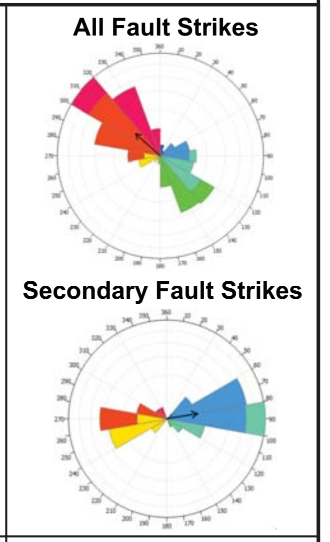

Map view of all faults mapped in the subsurface. Fault surfaces are colored to represent strike orientations. Pink dashed line represents the maximum extent of 3D seismic data.

In general, the strike values are dominantly northwest-southeast with an average orientation of 310 degrees. However, a secondary strike orientation is present in the northwestern corner of the fault array. This orientation is highlighted by yellow and green faults, with associated strikes trending east-northeast and west-northwest.

- Dominant strike: NW - SE
- Average strike orientation: (310 degrees)

- Secondary Strike: ENE - WNW
- Average strike orientation: (070 degrees)

Dip Angles

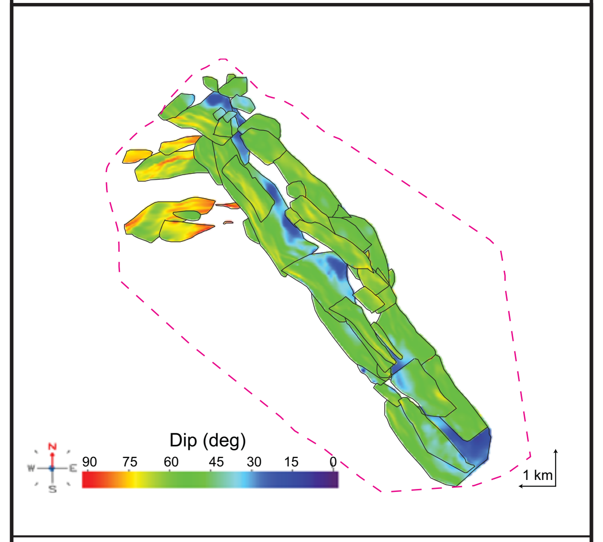

Map view of all fault surfaces that are colored to represent dip angle. Dip values in subsurface array vary spatially and vertically.

In General:

- NW-E
- NW-W } **can** be listric
- WSW-N
- ENE-S } **are** high angle

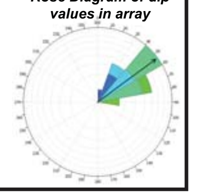

Rose Diagram of dip values in array

Throw Distribution

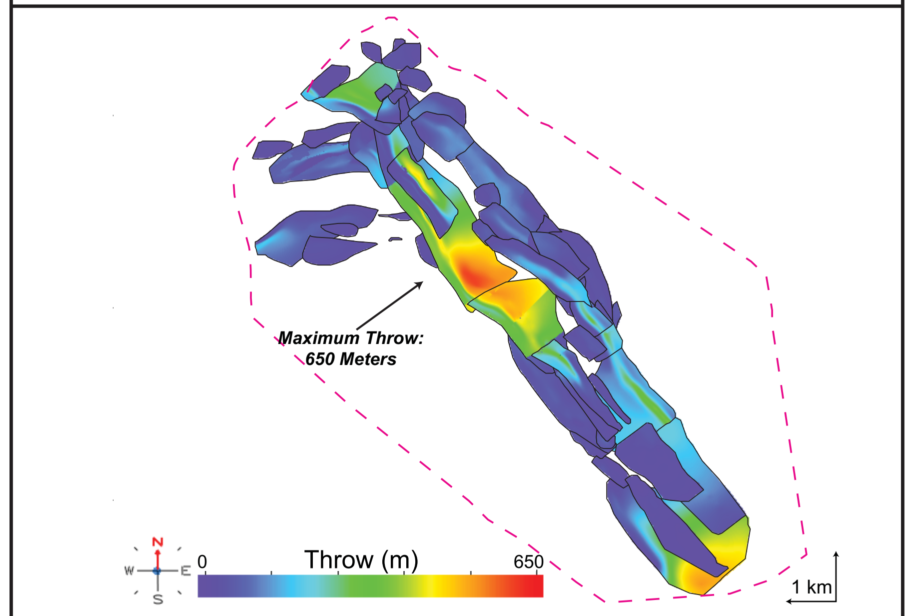

Map view of all faults mapped in the subsurface, fault surfaces are colored based on maximum throw on the fault; all fault surfaces are colored to the same scale

Throw is achieved primarily along northwest-southeast trending faults and is distributed along faultlinkage zones. Maximum throw within the fault array (640m) occurs on a NW-E dipping fault zone.

Fault Throw Analyses Results

Throw Distribution within Fault Zones

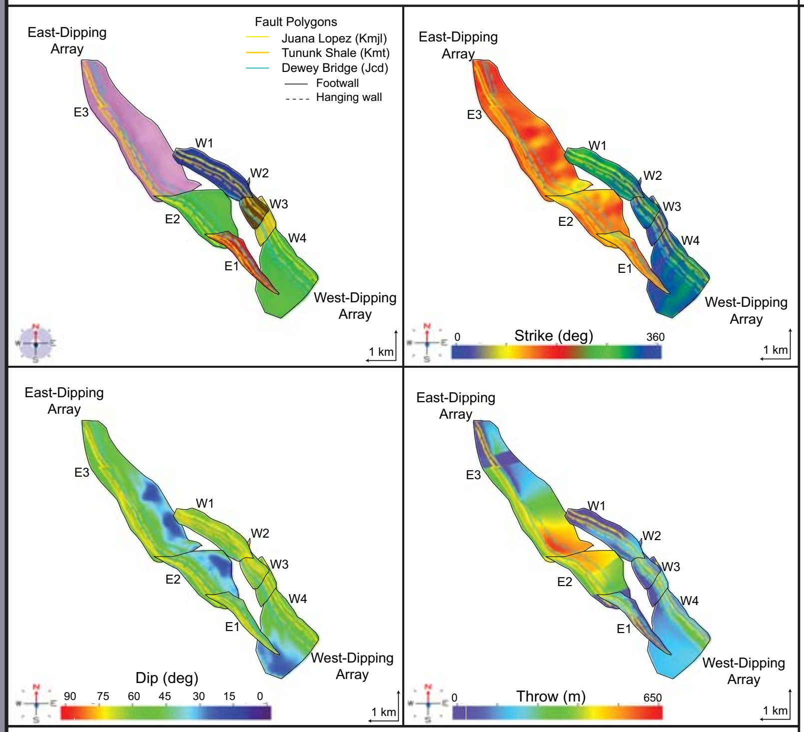

Map view of the two arrays that have been selected for in-detail static structural analyses. Each image shows fault surfaces that are colored to represent different attributes (individual fault segment, strike orientation, dip angles, and throw values).

Yellow, orange and teal polylines represent individual triangulated fault surfaces, solid and dashed lines represent the footwall and hanging wall cutoffs for the key stratigraphic horizons that were deformed while faulting

East-Dipping Fault Zone

Seismic Profiles along East-Dipping Array

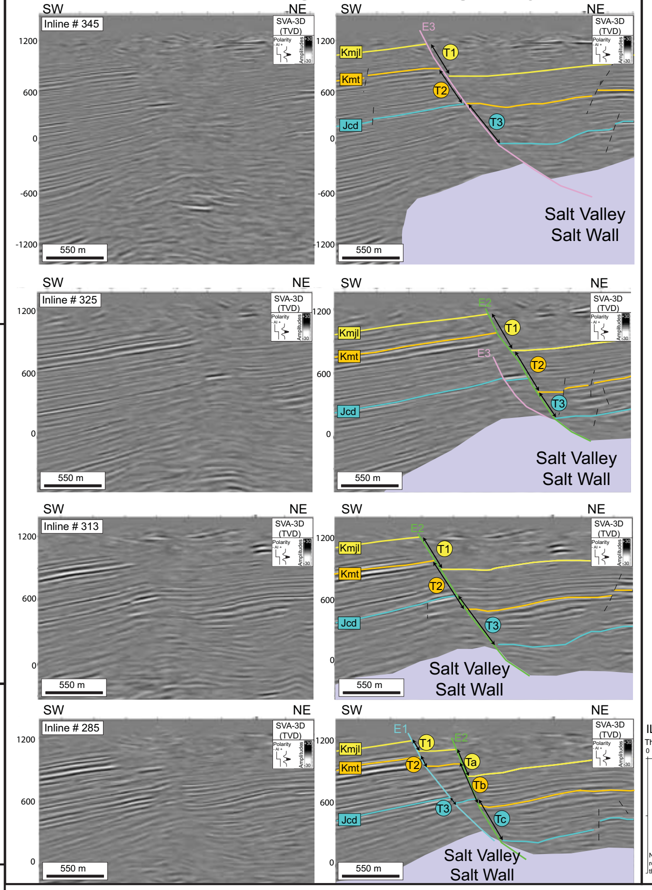

T-z crossplots

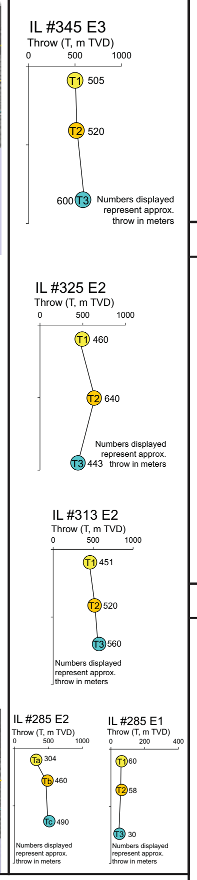

Four seismic inlines were analyzed to capture the geometric heterogeneities of the east-dipping fault zone. Each figure contains three parts: (a) clean seismic profile; (b) interpretation; and (c) T-z (Throw vs. depth) crossplots of the fault surfaces at three stratigraphic intervals. This fault zone is composed of three fault segments, E1-E3. Along-strike analysis of fault surface dip show that the east-dipping fault zone has a planar fault tip to the southeast and gradually develops a listric geometry in segments E2 and E3, where they are interpreted to detach on salt.

Segment E3 Throw Distribution

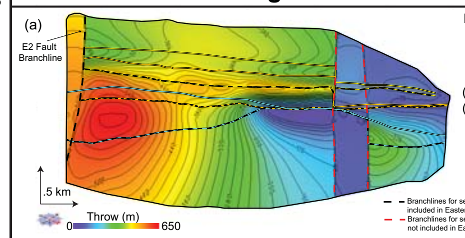

Fault segment E3 has a significant throw variation along strike. These variabilities in throw are attributed to displacement transfer between intersecting faults. These intersections are shown as dashed "branchlines".

(a) Contoured throw on the E1 fault with annotated contacts.
(b) E1 Throw-Distance (T-x) crossplot.

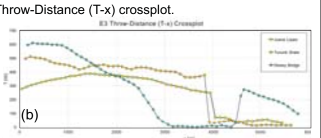

Segment E2 Throw Distribution

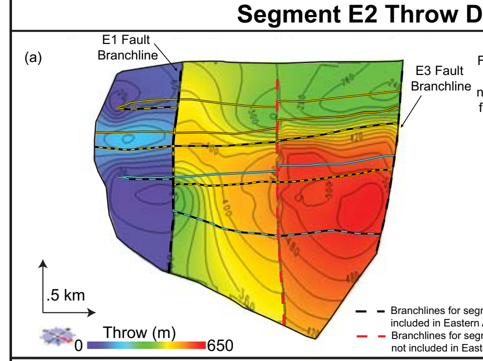

Fault segment E2 is the shortest segment in the fault zone. This fault surface connects the southern fault, E1 to the northwestern E3 fault surface. The southwestern end of the fault has radically lower throw than the rest of the surface,, which can be attributed to early fault segment linkup between E1 and E2.

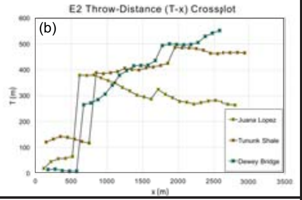

Segment E1 Throw Distribution

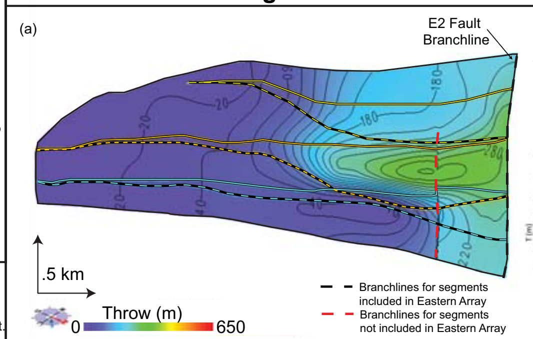

The southeastern tip of the fault is the shortest fault height (z), increasing to the northwest, coincident with throw least in the southeast, increasing to the northwest.

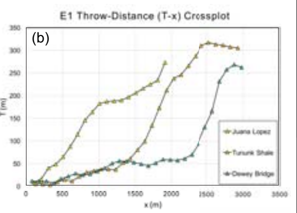

West-Dipping Fault Zone

Seismic Profiles along West-Dipping Array

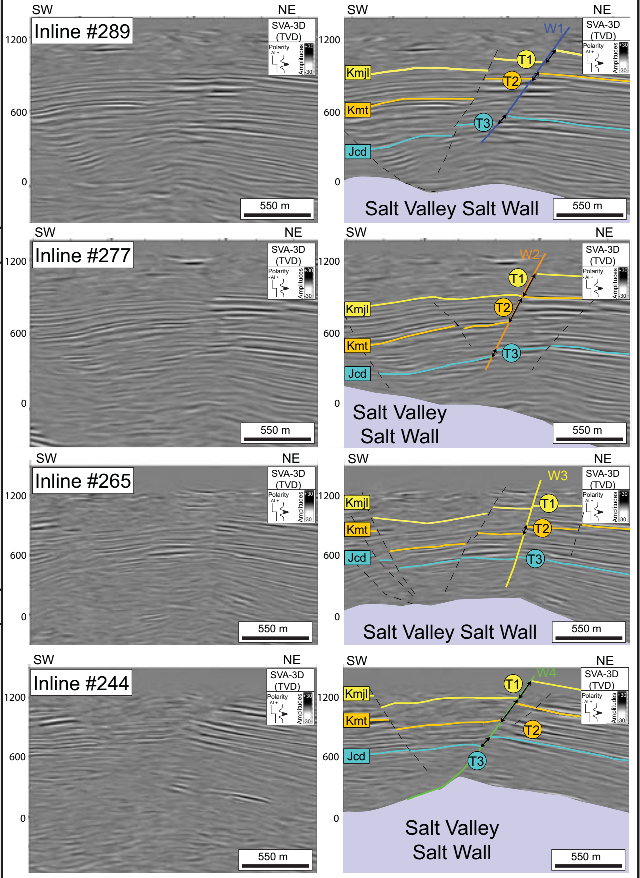

T-z crossplots

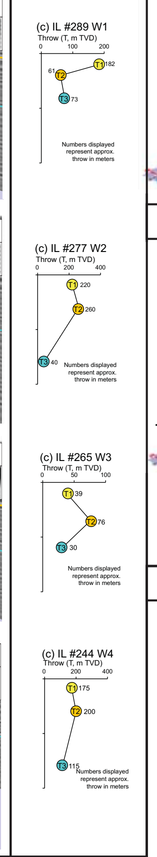

Four seismic inlines were analyzed to capture the geometric heterogeneities of the west-dipping fault zone. Each figure contains three parts: (a) clean seismic profile; (b) interpretation; and (c) T-z (Throw vs. depth) crossplots of the fault surfaces at three stratigraphic intervals. This fault zone is composed of four fault segments, W1-W4. Along-strike analysis of fault surface dip show that the West-dipping fault zone has a planar fault tip to the northwest, and only shows a listric geometry on the final fault segment, W4.

Segment W1 Throw Distribution

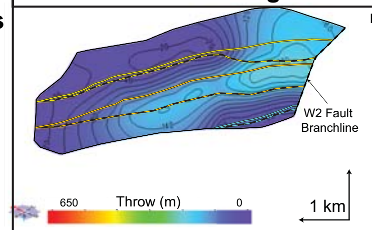

Fault segment W1 is the longest fault segment within the west-dipping fault array, however, significant vertical offset is not achieved along this fault. Notably, throw gradually increases along the length of the fault, with maximum displacement to the southeast.

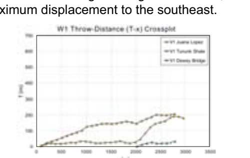

Segment W2 & W3 Throw Distribution

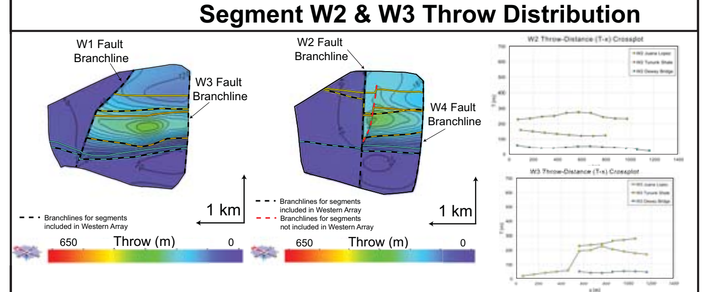

Fault segments W2 and W3 have similar dimensions (1.2 km long) as well as fault throw values. These segments make up the middle of the west-dipping array, and contain slightly more through than segment W1 and display throw compartmentalization. The greatest amount of throw is within the Tununk Shale Member, followed by the Juana Lopez Member for both segments.

Segment W4 Throw Distribution

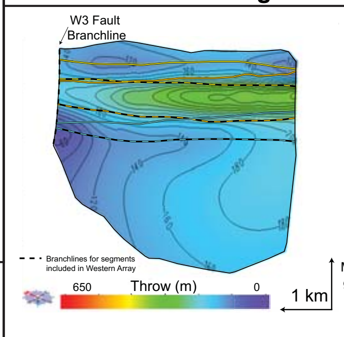

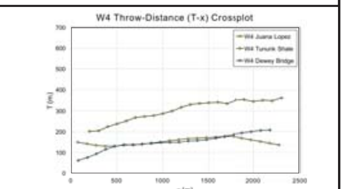

The southeastern-most fault segment of the west-dipping fault zone is W4. This segment is approximately 3.2 km long (x). The throws measured at the three stratigraphic sections remain consistent along the length of the fault. Maximum throw is measured on the Tununk Shale Member, gradually increasing from northwest to southeast, 200- 400 meters, respectively. The Juana Lopez and Dewey Bridge members both hover between throws of 75-200 meters along the faults length

East-Dipping Fault Zone

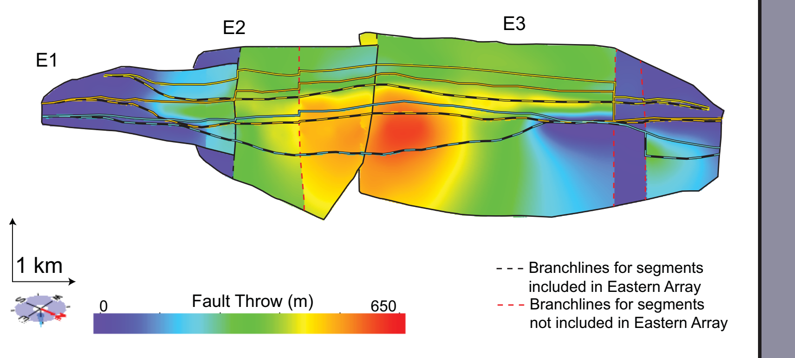

West-Dipping Fault Zone

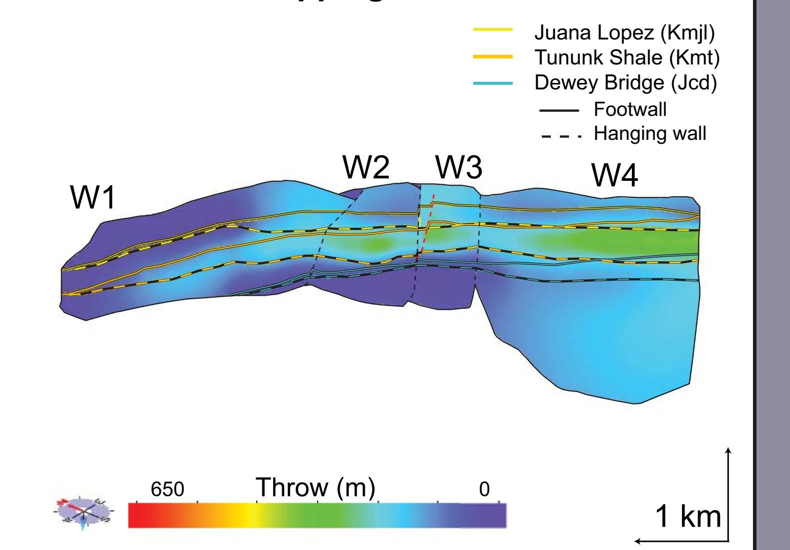

Field Results

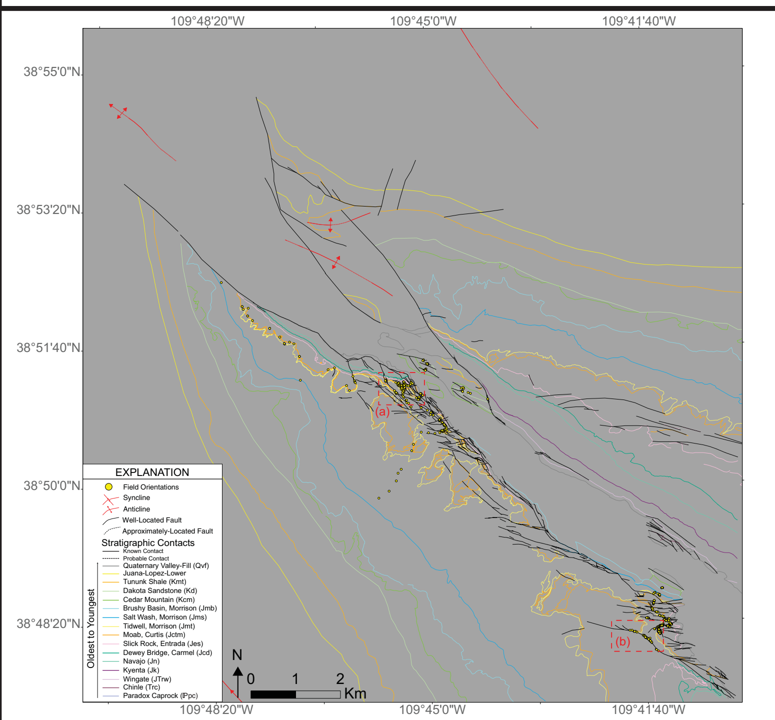

Comprehensive map of the surficially expressed geologic architecture of the northern Salt Valley salt wall. Colored lines represent the top-surface of each geologic unit, black lines define the traces of outcropping faults. Yellow circles represent locations of field measurements, used to conduct kinematic analyses.

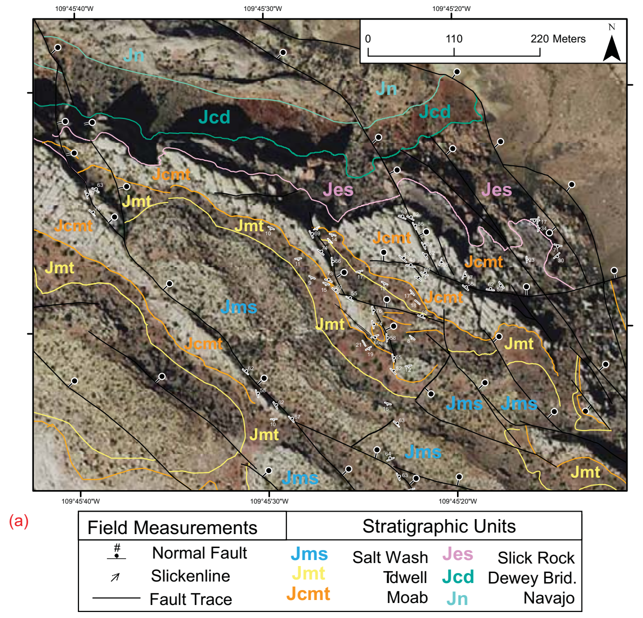

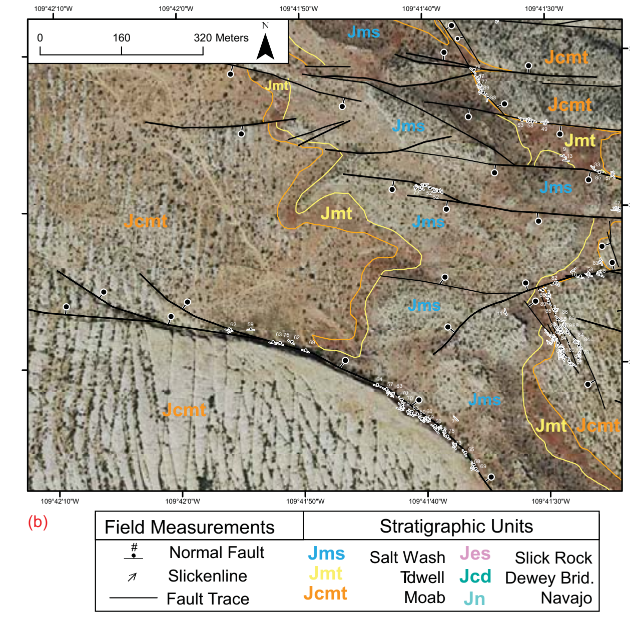

Inset maps highlighting field measurements collected in the (a) northern (b) southern regions of the field area.

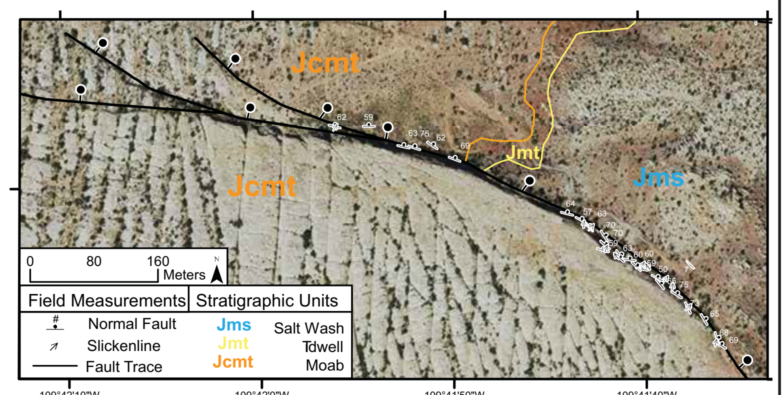

Zoom-in to inset (b) highlighting the fault used for the NW-E kinematic analysis. Fault orientations are shown in black symbols, outlined in white. Slickenline arrows point in direction of plunge. Fault plane dip orientations are labeled in white.

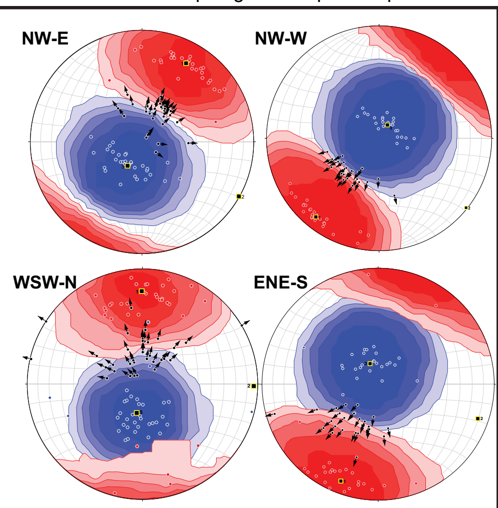

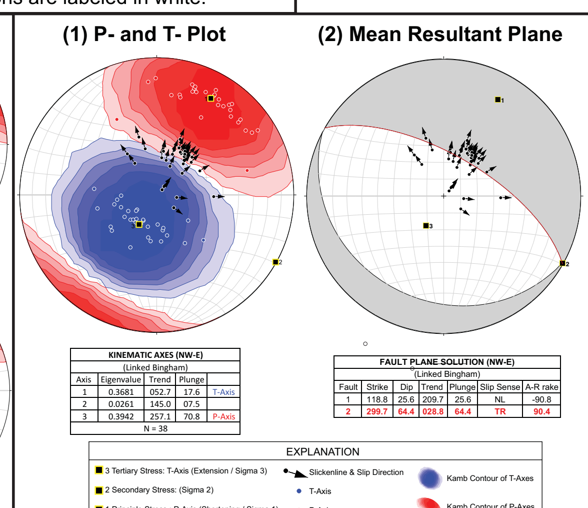

Kinematic Axes

Equal area stereonets displaying:
(1) P- and T- axes of faults orientations
(2) Mean resultant plane for the fault shown in map.

Hanging wall movement vectors are shown as black arrows in both plots.

In general, this fault:

- Has a lot of variation in orientation
- Shows combination of dip-slip and oblique slip motion

Mean resultant plane stereonet reveals oblique movement along fault

Synthesis of Field and Subsurface Results

Regional Observations

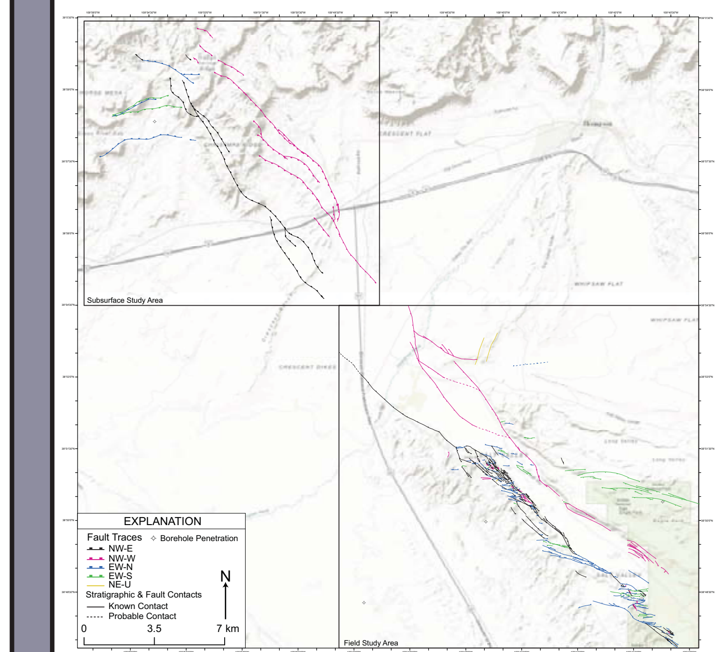

Composite map showing fault families, highlighted in different colors to accentuate the variability in orientations

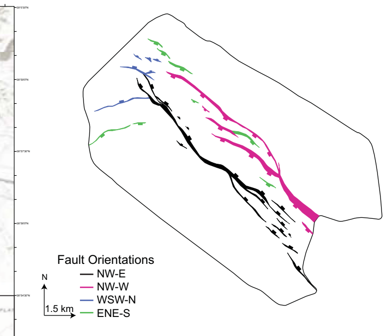

Zoom in to subsurface study area:
Orientations of faults that intersect the Tununk Shale Member of the Cretaceous Mancos Formation.

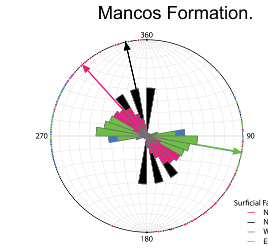

Rose diagram showing the trends of surficially-mapped faults. Colored arrows signify the mean vector of the four main fault trends

Regional Observations:

- Dominant fault fabric is NW-SE striking, dipping E and W
  - These are the longest faults with greatest throws
  - Are mapped at the highest frequency both in the field and in the subsurface
  - Orientation of underlying salt wall is subparallel to these faults
- E-W striking faults are present off the crest of the salt wall in the subsurface dataset

Fault Statistics

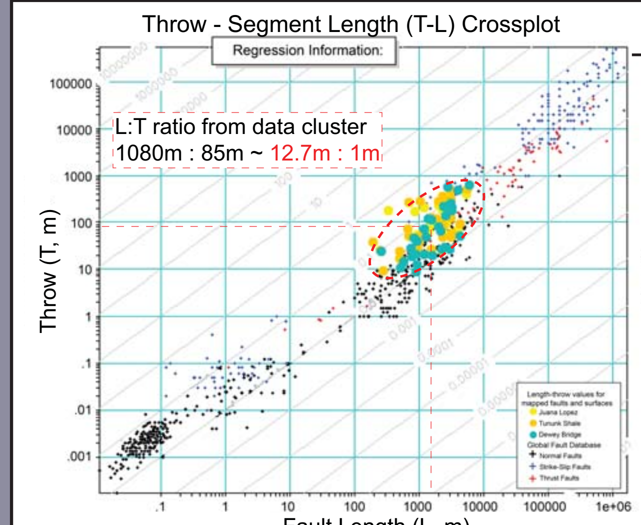

Throw- Segment Length (T-L) cross-plot showing where the subsurface faults plot with respect to the global fault database. Compared to the global normal fault dataset, the faults mapped in the subsurface portion of this study are somewhat over-displaced with an approximately 13:1 rather than 30:1 length vs. throw ratio.

Over-displacement of faults can be caused by one or a combination of two mechanisms: (1) enhancement of fault throw; (2) an element that can inhibit lateral fault propagation. In order to determine if one or both of these mechanisms may be affecting this fault system, we can refer to previous work completed on normal faults in the world, and to more local studies.

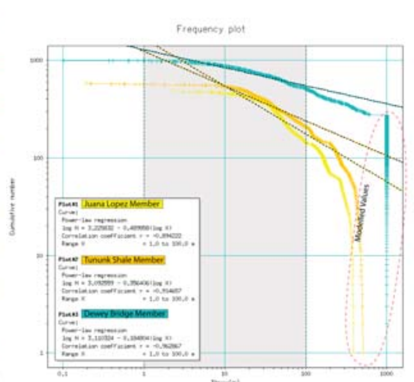

Cross plot of the frequency of faults within each stratigraphic unit that have various throw values. Best fit slope for each unit defines fault length population, shown by dashed straight lines.

Modeled fault numbers are not present throughout the entire fault array, but only present in locations of cross-cutting fault zones.

This discrepancy alludes to this array evolving from more local, compartmentalized strain (i.e. salt movement) rather than a uniform strain distribution that would be caused by regional extension. Thus, this graph cannot be used to predict the frequency of low-throw faults.

Crestal Geometry of the Salt Valley Salt Wall: Surface Asymmetries

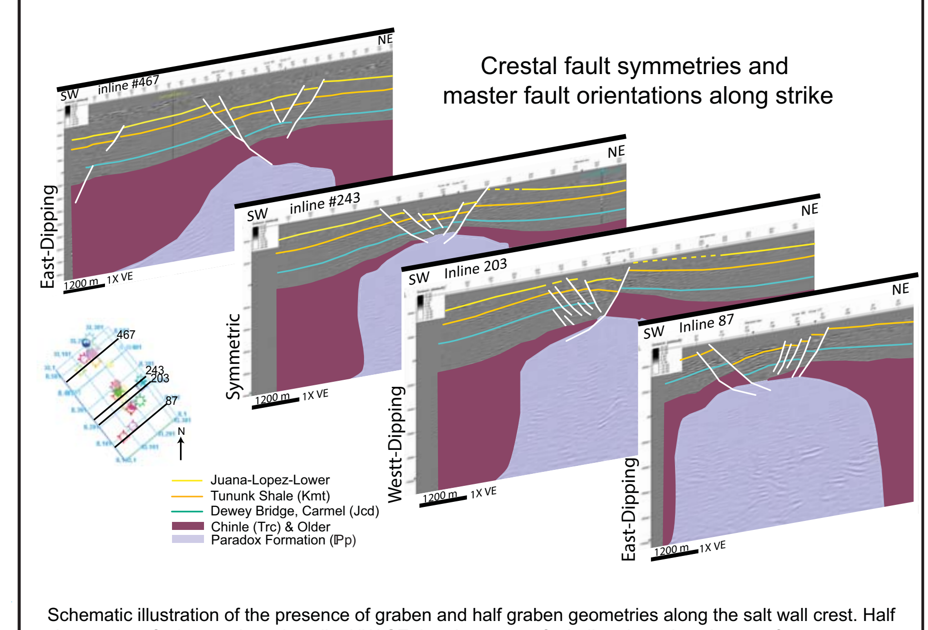

Schematic illustration of the presence of graben and half graben geometries along the salt wall crest. Half graben master faults consistently strike NW-SE, but the master-fault dip orientation changes from east to west dipping. Each seismic profile represents the same vertical and horizontal scale with no vertical exaggeration.

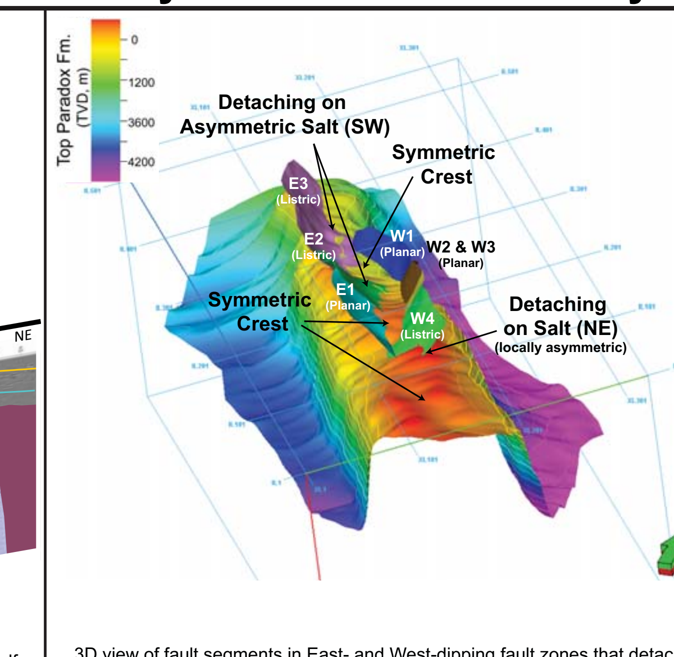

3D view of fault segments in East- and West-dipping fault zones that detach downward onto the Top Paradox Salt surface. Labels highlight regions where the crest of the Top-Paradox Salt is symmetric and asymmetric.

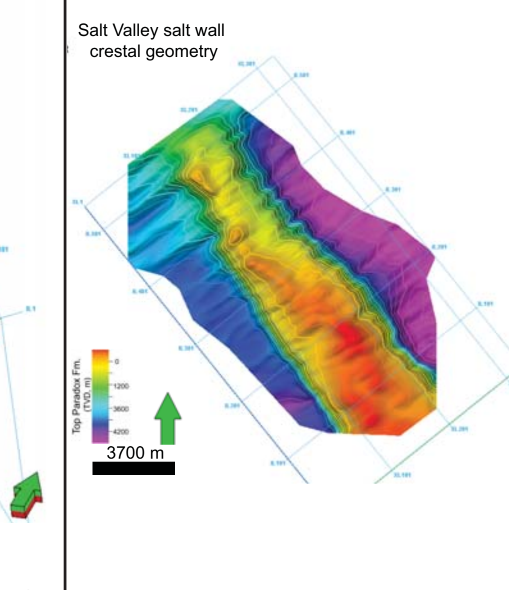

Map view of top-Paradox Salt surface. Surface asymmetries are visible from this view.

Crestal Geometry of the Salt Valley Salt Wall: Plunge

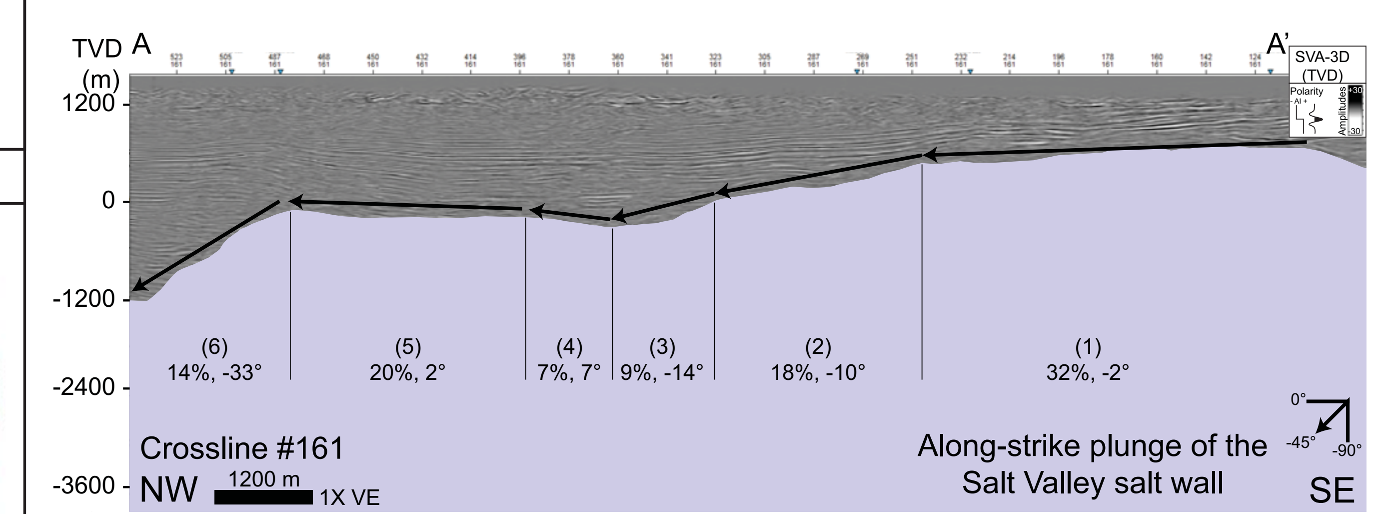

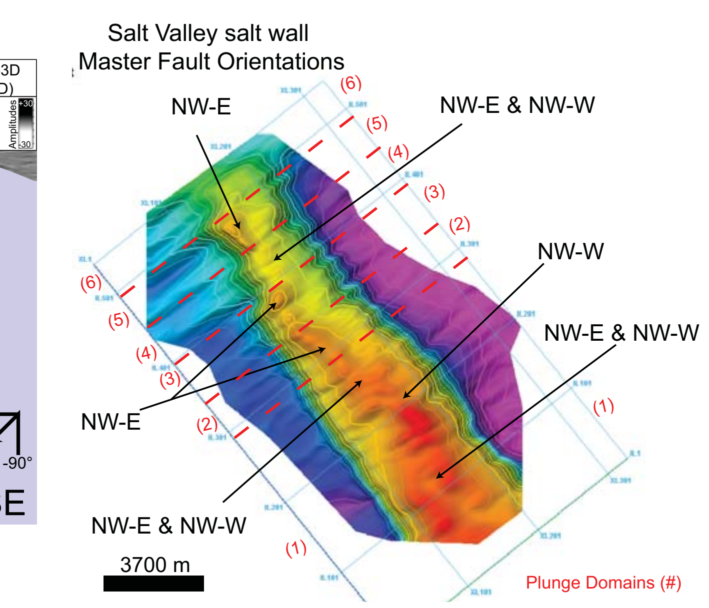

Seismic profile of the along-strike plunge variation of the Salt Valley salt wall. The top-Paradox Salt plunges gently to the northwest and can be easily broken into 6 do-

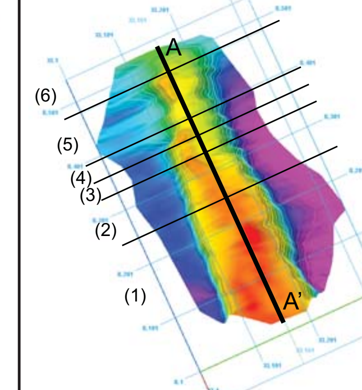

Plunge Domains of the Crest of the Salt Valley Salt Wall

(1) southeastern-most domain covers 32% of the length of the salt wall, with an average plunge of 2 degrees to the northwest.
(2) & (3) down-dip trend with increasing plunges of 10° to 14°, for 18% and 9% of the salt wall, respectively.
(4) & (5) Gain in elevation, with an initial incline of 7° shallowing out at 2° for 7% and 20% of the top-salt length, respectively.
(6) Abrupt change in plunge for the remaining 14% of the top-salt crest, plunging 33° to the northwest.

Plunge Domains vs. Master Fault Dip Direction

(1) Symmetric Crest: graben fault pattern
(2) Asymmetric Crest: half-graben east-dipping master fault
(3) Asymmetric Crest: half-graben east-dipping master fault
(4) Symmetric Crest: graben fault pattern
(5) Asymmetric Crest: half-graben east-dipping master fault
(6) Faults do not detach on salt, fault pattern is dominated by north- and south-dipping faults

Fault Growth

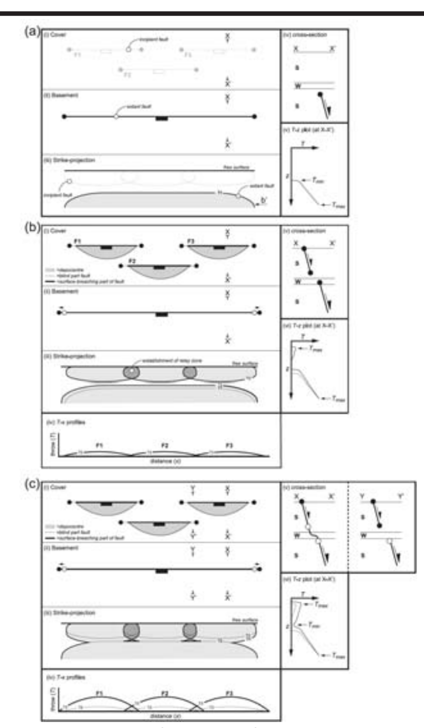

This research has focused on characterizing the geometric arrangement, nucleation, and evolution of a supra-salt fault array in the northern Paradox Basin.

There are two overarching controls that have influenced the nucleation and growth of the supra-salt fault array, the first being the role of salt, and the second being the influence of inherited structures.

Based on observations from this research, the faults with the greatest throws are listric in geometry and detach onto Top Paradox Salt. These faults nucleated as a response to localized strain from withdrawal and/or dissolution of the underlying salt wall. In present day, these faults are over-displaced.

A hypothesis for the development of this over-displacement is that fault growth initiated according to the isolated fault model, but asymmetries in the crestal geometry of the Paradox Salt created localized strain, creating heterogeneous fault geometries, and barriers in lateral fault growth, causing link-up early in growth history. Once linked, these fault linkages grew in accordance to the coherent fault growth model. This hybrid fault growth model has been described previously by (Jackson and Rotevatn, 2013). These faults are likely still active in present time, due to local salt dissolution and subsequent collapse of the salt wall.

The initiation of supra-salt faulting of the Salt Valley likely began with the transgression of the Cretaceous Interior Seaway, where marine waters interacted with the shallow body of Paradox Salt, causing salt dissolution. The crestal subsidence of the salt wall from dissolution was magnified by local depositional thickening of Cretaceous aged sediments, which can be seen in several seismic profiles.

A schematic illustration of the coherent fault model, showing salt and dip-linkage on fault growth. (a) Time 1 = establishment of a mature normal fault system below the mechanically-weak layer (ii=iv). T-z profile is characterized by a progressive upward decrease in throw to the upper tip (v); (b) Time 2 = dip-slip reactivation of the lower fault system. Nucleation and rapid lengthening of the upper fault system; interaction with the free surface may result in the formation of a growth fault-bound depocentre (i, iii and iv); (c) Time 3 (T3) = downward propagation of the upper fault system occurs despite 'pinning' of the lateral fault tips (iii, v and vi). Depocentre geometry and size remains fixed (i). The upper and lower fault systems may breach the mechanically-weak layer at this time, resulting in the formation of a fault surface that is characterized by a single structure at depth and multiple structures at shallower depths (iii, v and iv).W¼ 'weak' layers (i.e. salt); S ¼ 'strong' layers. Tmax ¼ throw maximum;Tmin ¼ throw minimum. Figure and caption taken from Jackson and Rotevatn, 2013.

Role of Inherited Structures

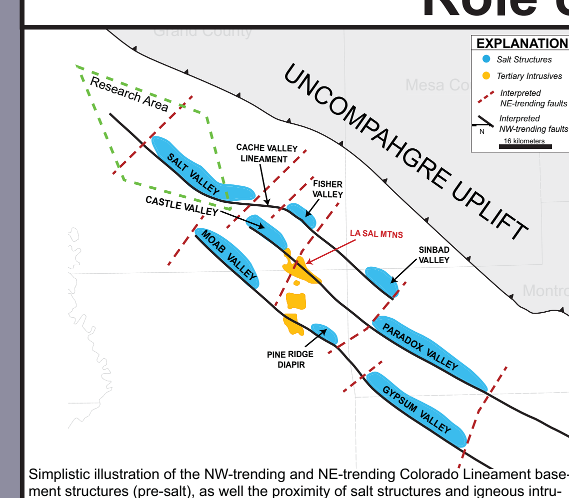

Simplistic illustration of the NW-trending and NE-trending Colorado Lineament basement structures (pre-salt), as well the proximity of salt structures and igneous intrusions. Green dashed polygon represents the approximate location for this research (modified from Lehmann, 2015).

Basement-involved faults have influenced many structures within the Paradox Basin, including the locations and orientations of the elongate salt walls and could potentially control the locations of supra-salt faulting.

The dominant northwest-southeast structural trends documented throughout the Paradox Basin have been attributed to Mississippian-aged flexural normal faults which deform crystalline basement and pre-Paradox stratigraphic section (Barbeau, 2003). These basement-involved faults have been interpreted to act as basinward-flow barriers, for the elongate evaporitic salt walls in the basin

In addition to this NW-SE trending fault system, magnetic data, seismic reflection data, as well as published work have suggested that there is a secondary basement fabric that may have significant control on the placement of salt within the Paradox Basin. Specifically, this secondary fabric is thought to control the northwestern and southeastern lateral terminations of the elongate salt walls.

These underlying ENE-SWS trending basement fabric influences the locations of salt wall terminations, and may also inhibit lateral salt flow within the salt walls, which can be applied to the Salt Valley salt wall.

References

Barbeau, D. L., 2003, A flexural model for the Paradox Basin: implications for the tectonics of the Ancestral Rocky Mountains: Basin Research, v. 15, p. 97–115.
Doelling, H. H., 1983, Observations on Paradox Basin salt anticlines: 81-90 p.
Giles, K. a, and T. F. Lawton, 2002, stratigraphy adjacent northeastern Mexico: October, v. 5, no. 5, p. 823–840.
Hearon IV, T. E., 2013, Analysis of salt-sediment interaction associated with steep diapirs and allochthonous salt: Flinders and Willouran ranges, south Australia, and the deepwater northern gulf of Mexico: p. 178.
Hudec, M. R., and M. P. A. Jackson, 2007, Terra infirma: Understanding salt tectonics: Earth-Science Reviews, v. 82, no. 1, p. 1–28, doi:10.1016/j.earscirev.2007.01.001.
Jackson, C. A. L., and A. Rotevatn, 2013, 3D seismic analysis of the structure and evolution of a salt-influenced normal fault zone: A test of competing fault growth models: Journal of Structural Geology, v. 54, p. 215–234, doi:10.1016/j.jsg.2013.06.012.
Kluth, C. F., and H. R. Duchene, 2009, Late Pennsylvanian and Early Permian Structural Geology and Tectonic History of the Paradox Basin and Uncompahgre Uplift, Colorado and Utah: RMAG Special Publication, v. The Parado, p. 178–197.
Lehmann, K., 2015, Three-Dimentional Modeling of Complex Salt Wall Terminations in the Paradox Basin: Implications for Salt Structure Evolution, Compartmentalizing Fault Trends and Petroleum Exploration: Colorado School of Mines, doi:10.1017/CBO9781107415324.004.
Morley, C. K., S. Back, P. Van Rensbergen, P. Crevello, and J. J. Lambiase, 2003, Characteristics of repeated, detached, Miocene–Pliocene tectonic inversion events, in a large delta province on an active margin, Brunei Darussalam, Borneo: Journal of Structural Geology, v. 25, no. 7, p. 1147–1169, doi:10.1016/S0191-8141(02)00130-X.
Richardson, N. J., J. R. Underhill, and G. Lewis, 2005, The role of evaporite mobility in modifying subsidence patterns during normal fault growth and linkage, Halten Terrace, Mid-Norway: Basin Research, v. 17, no. 2, p. 203–223, doi:10.1111/j.1365-2117.2005.00250.x.
Stevenson, G. M., and L. L. Wray, 2009, History of Petroleum Exploration of Paleozoic Targets in the Paradox Basin: no. 1, p. 1–23.
Trudgill, B. D., 2011, The Influence of "Mobile" Evaporite Distribution on Salt Wall Growth and Stratigraphic Architecture in the Northern Paradox Basin, Southeastern Utah: Basin Research, v. 23, no. 2, p. 208–238, doi:10.1111/j.1365-2117.2010.00478.x.
Trudgill, B. D., and W. C. Arbuckle, 2009, Reservoir Characterization of Clastic Cycle Sequences in the Paradox Formation of the Hermosa Group , Paradox Basin , Utah.
Trudgill, B. D., and J. Cartwright, 1994, Relay-ramp forms and normal-fault linkages, Canyonlands National Park, Utah: Geological Society of America Bulletin, v. 106, no. 9, p. 1143–1157, doi:10.1130/0016-7606(1994)106<1143:RRFANF>2.3.CO;2.
Tvedt, A. B. M., A. Rotevatn, C. A. L. Jackson, H. Fossen, and R. L. Gawthorpe, 2013, Growth of normal faults in multilayer sequences: A 3D seismic case study from the Egersund Basin, Norwegian North Sea: Journal of Structural Geology, v. 55, p. 1–20, doi:10.1016/j.jsg.2013.08.002.

Conclusions

Research conducted on the Salt Valley supra-salt fault array have resulted in:

- The identification of four dominant fault orientations, present throughout the entirety of the research area.
- The generation of a 3D structural framework of the Salt Valley's supra-salt fault system constrained by 3D seismic reflection survey and borehole penetrations.
- The execution of quantitative analyses (e.g., fault throw-length (T-L); throw-distance (T-x); throw-depth (T-z); and throw variation along strike and between stratigraphic intervals) to determine the complex fault segment linkage history of the supra-salt fault system.
- The construction of a more-accurate sub-regional geologic contact map of the northwestern Salt Valley, which incorporates published data points, digitally-collected field measurements, as well as the creation several small-scale inset maps highlighting fault zones studied in advanced analyses.
- The completion of kinematic analyses of digitally-collected outcropping faults.
- The interpretation for the nucleation, fault growth evolution, and mechanism of formation for the supra-salt fault system, based on observations from both field and subsurface results.
- The northwestern tip of the Salt Valley salt wall likely coincides with the location of an underlying ENE-SWS trending Proterozoic basement fabric, similar to other salt wall terminations mapped in the Paradox Basin.